Korean J. Chem. Eng., 34(2), 440-453 (2017)
DOI: 10.1007/s11814-016-0269-1

pISSN: 0256-1115
eISSN: 1975-7220

High speed spin coating in fabrication of Pebax 1657 based mixed matrix membrane filled with ultra-porous ZIF-8 particles for CO_2/CH_4 separation

Abolfazl Jomekian*,, Reza Mosayebi Behbahani*,†, Toraj Mohammadi**, and Ali Kargari*****

*Gas Engineering Department, Ahvaz Faculty of Petroleum Engineering, Petroleum University of Technology (PUT), P. O. Box 63431, Ahvaz, Iran
**Faculty of Chemical Engineering, Iran University of Science and Technology (IUST), Narmak, Tehran, Iran
***Department of Petrochemical Engineering, Amirkabir University of Technology (AUT), Mahshahr, Iran
(*Received 30 June 2016 • accepted 25 September 2016*)

Abstract−Modified ultra-porous ZIF-8 particles were used to prepare novel ZIF-8/Pebax 1657 mixed matrix membranes (MMMs) on PES support for separation of CO_2 from CH_4 using spin coating method. TEM and SEM were used to characterize modified ZIF-8 particles. SEM was also used to investigate the morphology of synthesized MMMs. The MMMs with thinner selective layer showed higher CO_2 permeability and lower CO_2/CH_4 selectivity in permeation tests compared to MMMs with thicker selective layer. The plasticization was recognized as the main reason for rise in CO_2 permeability and drop in CO_2/CH_4 selectivity of thinner MMMs. The gas sorption results showed that the high permeability of CO_2 in MMMs is mainly due to the high solubility of this gas in MMMs, leading to high CO_2/CH_4 solubility selectivity for MMMs. The fractional free volume and void volume fraction of MMMs increased as the thickness of membrane decreased. Applying higher mixed feed pressures and permeation tests temperatures resulted in increase in CO_2 permeability and decrease in CO_2/CH_4 selectivity. At highest testing temperature (60 °C), the CO_2 permeability of synthesized MMMs with thinner selective layer remarkably increased.

Keywords: ZIF-8, Modification, Pebax 1657, Spin Coating, CO_2 Separation

INTRODUCTION

Natural gas sweetening is one of the major operations in the natural gas treatment process. The aim of natural gas sweetening is to separate hydrocarbons (mainly CH_4) from hazardous and acidic impurities (mainly CO_2) [1]. The absorption of acid gases by alcohol amines, distillation and cryogenic operations is currently ongoing in many industrial gas plants as the main operations for sweetening and treatment of natural gas [2-7]. However, absorption, evaporation and liquefaction all consume considerable amount of energy, therefore, the need for novel, energy efficient and effective methods for natural gas sweetening was recognized by industry [8,9].

Polymeric membranes have emerged as promising candidates for this purpose. They are flexible, cheap and energy efficient, but they suffer from the lack of enough performance in separation of gases [8,9]. This is mainly due to the opposite behavior of their permeability and selectivity as it was observed in many researches and summarized by Robeson in 2008 [10]. One approach to resolve this problem is to combine the flexibility of polymers with mechanical stability and separation performance of inorganic materials by synthesizing a new type of membranes, the so-called mixed matrix membranes (MMMs). These types of membranes usually consist of a polymer as matrix (host) and an inorganic material as filler (guest) merged into a shape of a thin uniform film. These membranes were extensively investigated in all membrane separation process fields, especially in gas separation [11-14]. There are many reports available in the literature related to gas separation by MMMs prepared with different combinations of organic and inorganic phases [9,11-13,15,16].

Separation of CO_2 from gases by MMMs synthesized by block copolymers has attracted a lot of attention in recent years [17,18]. Polyether block amide, a multiblock copolymer with trade name of Pebax which consists of polyethers (PEO or PTMO) as soft segments and polyamides (PA6 or PA12) as hard segments, has been used more than other types of copolymers for CO_2 separation [19-35]. Various types of inorganic and organic materials such as nanosilica and H-Mordenite [28], POSS [34], silica [36], carbon nanotube [29], ceramics [20] and zeolite 4A [37] have been introduced in the matrix of Pebax to enhance its CO_2 separation performance.

Zeolitic imidazolate frameworks (ZIFs), a sub-class of metal organic frameworks (MOFs) have been extensively investigated in the shape of inorganic membranes or MMMs for separation of gases [11,13,27,30,38-46]. ZIF-8 is one the most studied members of this family. It has attracted attention as a high potential adsorbent for CO_2 in MMMs due to its intrinsic affinity for this gas [11,30,39,40,42]. According to Cravillon et al. [47] the formation of microporous ZIF-8 has two possible mechanisms. The clusters generated from precursors turn into either a crystalline nucleus or an amorphous nucleus; then the resulting nucleus grows to become a ZIF-8 nanocrystal. ZIF-8 crystals have been synthesized by several different methods, such as solvothermal, microwave assisted,

†To whom correspondence should be addressed.
E-mail: behbahani@put.ac.ir, r_behbahani@yahoo.com
Copyright by The Korean Institute of Chemical Engineers.

sonochemical and mechanochemical, and dry-gel conversion methods [41]. The diversity of synthesis routes resulted in formation of ZIF-8 crystals with different particle sizes and surface areas. However, the ZIF-8 pores kept their microporosity (pore size≈0.34 nm) during synthesis regardless of the applied method. Although microporous ZIFs exhibit high surface areas, their structure limits mass transfer through pores, leading to deterioration of their performance in application involving molecular transportation [48]. This drawback can be overcome by modification of the pore size of ZIFs by incorporation of structural modifiers such as templates into the synthesis procedure. Accordingly, the modification of ZIF-8 pore size for a specific application is widely investigated and reported [38,47,49-54]. One of the promising methods to adjust the pore size and surface area of ZIF-8 particles is to utilize copolymers as structure direction agent in synthesis. Cao et al. [48] utilized poly(styrene)-block-poly(4-vinylpyridine) and poly(styrene)-block-poly(acrylic acid) separately to enhance the pore size, pore volume and surface area of ZIF-8. The self-assembly of micelles leads to formation of a template which provides a mesoporous framework for ZIF-8 precursors (Zn^{2+} and MeIM). The removal of this template leads to formation of mesoporous ZIF-8 from assembled precursors. In similar approaches, amphiphilic block copolymers have been used for modification of pore structure of other types of MOFs as well [55-57].

The modification of pore size of ZIF-8 using poly(ether block amide) grade 1657 (Pebax 1657) as structure directing agent was recently conducted and reported by our group [58]. Hence, in this work, as first novel approach, previously synthesized and modified ZIF-8 particles with enhanced porosity were used as fillers in the matrix of Pebax 1657 for separation of CO_2 from CH_4. The enhanced porosity and pore size of templated ZIF-8 particles in the matrix of Pebax 1657 provides higher surface area for sorption of CO_2 compared to conventionally prepared ZIF-8, leading to enhancement of CO_2 permeability and CO_2/CH_4 selectivity compared with the state of the art Pebax based MMMs synthesized with different fillers such as zeolites, MOFs, and carbon nanotubes.

In fabrication of multilayer membranes, the thickness of the selective top-layer has a very important role in effective separation of penetrants. A defect-free thin selective top-layer is desired in every membrane synthesis procedure. However, in the case of Pebax 1657, due to the high viscosity of casting solution, using a casting bar often leads to formation of relatively thick layer, therefore coating has been used in many works instead of casting [20,21,28,30, 36,59,60]. Dip coating, which is the frequently used technique of coating, is not very efficient in coating of non-planar surfaces. The control of thickness is difficult in dip coating; therefore, the coated layer is not homogeneous [61]. On the other hand, spin coating, is effective for reproducible synthesis of coated thin layers with high structural uniformity. However, the reported spinning speeds that were used for coating in literature for fabrication of MMMs, generally are not higher than 600 rpm due to the formation of non-uniform selective surface in higher spinning speeds.

In this study, as second novel work, unconventional high spinning speeds (500-3,000 rpm) were applied for formation of selective top layer of ZIF-8/Pebax 1657 MMMs using a converted centrifugal separator as spin coater to reduce the defect free selective layer thickness as low as possible. The ZIF-8 particles which were used as fillers in this work were previously modified by the aid of Pebax 1657 as structure directing agent; the complete procedure of modification can be found in literature [58]. The CO_2/CH_4 separation performance of synthesized ZIF-8/Pebax 1657 MMMs on PES support was evaluated in both pure and mixed gas tests.

EXPERIMENTAL

1. Materials

2-methyl imidazole (99%, MeIm), zinc nitrate hexahydrate (99%, $Zn(NO_3)_2{\cdot}6H_2O$), methanol (99.99% MeOH), ethanol (99.99%, EtOH), dimethylformamide (99.99%, DMF), deionized water (H_2O) and normal-hexane (99.99%, n-hexane), were all purchased from Merck Inc. and used as received without further purification. Polyethersulfone (PES) and Pebax 1657 were provided by BASF Inc. and Arkema Inc. respectively.

2. Synthesis of ZIF-8 Particles

The ZIF-8 particles were synthesized by the method reported by Jomekian et al. [58]. A brief description of the procedure is provided here. The templating solution was prepared by dissolving different amount of Pebax 1657 in the mixture of 70 wt% EtOH and 30 wt% H_2O. This solution was used as structure directing agent in formation of ZIF-8 particles with enhanced porosity. To modify ZIF-8 crystals, the precursors (MeIM and $Zn(NO_3)_2{\cdot}6(H_2O)$) with different molar ratios (321/, 8/1 and 2/1) were dissolved separately in templating solution of Pebax 1657; then both solutions of precursors were mixed and stirred. The resulting mixed solution was placed into a Teflon-lined autoclave, boosting the assembly reactions of precursors. The template resulting from self-assembly was washed and then dried in an oven. The synthesis procedure was performed at different temperatures (30 °C, 45 °C and 60 °C) exactly as explained.

The ZIF-8 sample synthesized with MeIM/Zn^{2+}=2/1 at 60 °C showed the highest BET surface area (1,869 m^2/g) and relatively large crystal size (191 nm); however, the ZIF-8 sample synthesized with MeIM/Zn^{2+}=32/1 at 30 °C had smallest crystal size (43 nm) with a comparable BET surface area (1,694 m^2/g) [58]. Using spin coater to fabricate a very thin selective layer needs very small nanoparticles to avoid surface defects; therefore we selected ZIF-8 nanoparticles with smallest particles size to be used in Pebax 1657 matrix.

3. Preparation of ZIF-8/Pebax 1657 MMMs

To fabricate MMMs selective layer, Pebax 1657 was dissolved in a mixture of 70 wt% ethanol-30 wt% water. The solution was about 24 hours under vigorous stirring at 70 °C. As-synthesized ZIF-8 particles were suspended in a small amount of ethanol for wetting. This suspension was added to Pebax 1657 solution and vigorously stirred. The ultrasonic bath was successively applied to ensure the complete dispersion of ZIF-8 particles in the solution.

To fabricate a support sub-layer, 18 wt% of PES solution was prepared by dissolving predetermined amount of this polymer in DMF. Aging for hours to ensure the disappearance of air bubbles was necessary. This solution was cast on a glass substrate using a casting bar. After several minutes, the glass substrate was placed in a coagulation bath of water. About an hour was needed for the PES layer to coagulate and for phase inversion to complete. After

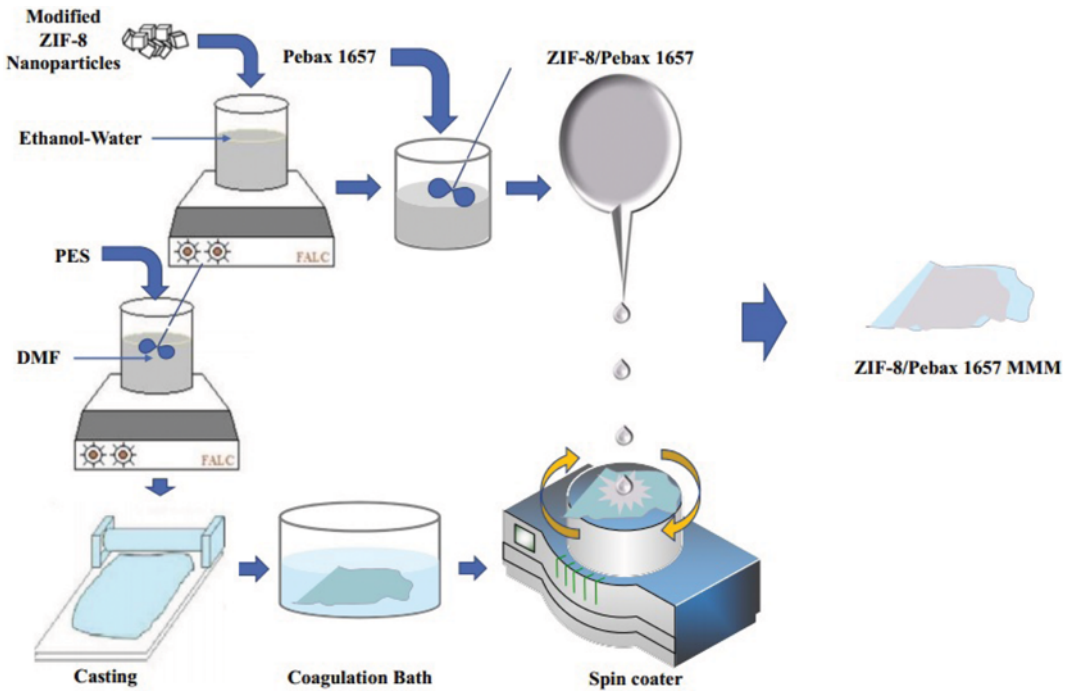

Fig. 1. The schematic diagram of preparation of ZIF-8/Pebax MMMs on PES support.

this duration, the PES film was separated from glass substrate and placed for 24 hours in air to dry.

To synthesize the ZIF-8/Pebax 1657 on PES support, initially the dried PES film was stocked on the spin coater (a customized centrifugal separator), then the synthesized solutions of ZIF-8/Pebax 1657 were poured dropwise on the surface of spinning PES support. The spinning speed was changed from 500 to 1,000, 2,000 and finally to 3,000 rpm to investigate the effect of spinning speed on the thickness of selective layer, and finally on the performance of fabricated MMM. A brief procedure of MMMs preparation is schematically presented in Fig. 1.

Table 1. The abbreviated names of all synthesized membranes

Abbreviated name of membranes	Coating method	ZIF-8 content (wt%)	Spinning speed (1,000 rpm)
Pure-SC*	Spin coating	0	0.5
SC-2-0.5	Spin coating	2	0.5
SC-4-0.5	Spin coating	4	0.5
SC-2-1	Spin coating	2	1
SC-4-1	Spin coating	4	1
SC-2-2	Spin coating	2	2
SC-4-2	Spin coating	4	2
SC-2-3	Spin coating	2	3
SC-4-3	Spin coating	4	3
Pure-DC**	Dip coating	0	-
DC-2	Dip coating	2	-
DC-4	Dip coating	4	-

*Spin coating
**Dip coating

The coating solution was synthesized by 2 wt% of Pebax 1657 in solvent to decrease the viscosity of solution and to facilitate the formation of thinner top layer in spin coating operation. Different loadings of ZIF-8 in the MMMs (2 and 4 wt%) were used to synthesize ZIF-8/Pebax 1657 MMMs. One pure Pebax 1657 membrane sample together with two MMM samples with loadings of 2 and 4 wt% of ZIF-8 in Pebax 1657 (2 wt%) were also synthesized by conventional dip coating method for comparison purpose. The abbreviated names of all synthesized and investigated membrane samples in this work are shown in Table 1.

4. Gas Permeation and Sorption Measurements

Gas permeation tests were performed using flat sheet module made of PTFE (Fig. 2) in a constant pressure variable volume setup (Fig. 3) in both pure and mixed gas conditions.

This setup was equipped with two mass flow controllers (Brooks

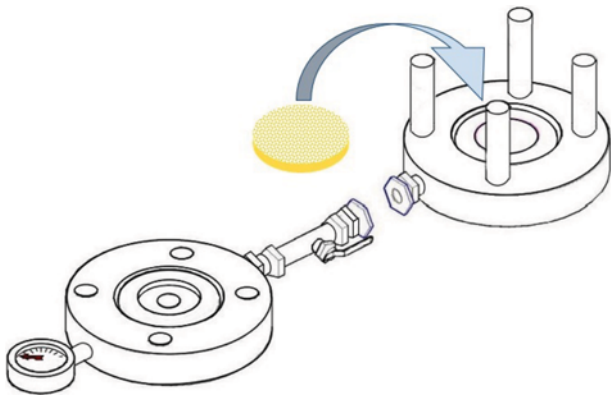

Fig. 2. Schematic diagram of gas permeation test module.

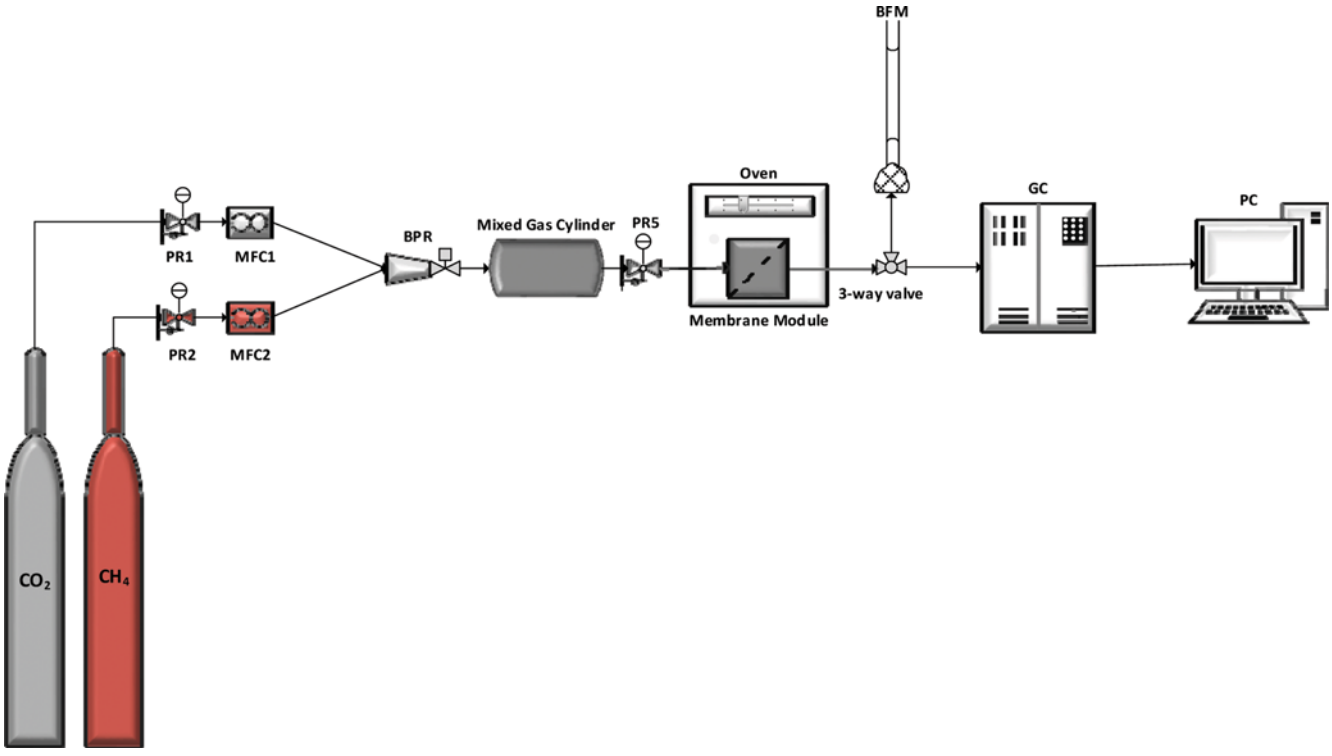

Fig. 3. Schematic diagram of mixed gas permeation test set-up.
PR. Pressure regulator
MFC. Mass flow controller
BPR. Back-pressure regulator
BFM. Bubble flow meter
GC. Gas chromatography
PC. Personal computer

5850 EM, US) for exact preparation of a feed mixture with desired gas compositions. A gas chromatograph (GC) (ACME 6100, Korea) equipped with a thermal conductivity detector (TCD) was used for exact determination of permeate composition. Helium was used as carrier gas to carry the investigated gases through the column into the GC. The permeation data for each membrane were collected from three distinct samples of that membrane which was synthesized by an exact similar procedure and the average and errors were reported.

The permeabilities of gases in pure and mixed gas tests were directly calculated from the gas flux data measured by bubble flow meter with the well-known defining Eq. (1):

$$P_i = \frac{Q \times l}{A \times (p_{fi} - p_{pi})} \quad (1)$$

where P_i is permeability coefficient (cm^3 (STP) cm/(s cm^2 cmHg)) of component i, Q_i is the volumetric flowrate of permeated component i (cm^3/s), l is the thickness of membrane selective layer (cm), A is the effective membrane area (cm^2) for gas permeation, and p_{fi} and p_{pi} are partial pressures of component i at feed and permeate side (cmHg), respectively.

The sorption tests were conducted on CO_2 and CH_4 gases with purity of 99.99% by the aid of a volumetric system (Gold APP Instruments, H-Sorb 2600). Before each test, the samples were degassed at 373 K for 6 h. The degassed samples then were cooled to 303 K with a decreasing rate of 1 K/min.

The solubility coefficients (S_i) of CO_2 and CH_4 in membranes were extracted from the obtained adsorption isotherms at temperature of 30 °C and pressure of 5 bar. The diffusivity coefficients (D_i) of CO_2 and CH_4 in membranes were calculated based on a well-stablished solution-diffusion model by the following equation:

$$D_i = \frac{P_i}{S_i} \quad (2)$$

The selectivity $\alpha_{A/B}$ is defined as the gas permeability ratio of more permeable gas (P_A) to that of the less permeable gas (P_B). It also can be expressed based on the product of solubility selectivity (S_A/S_B) and diffusivity selectivity (D_A/D_B) of these two gases:

$$\alpha_{A/B} = \frac{P_A}{P_B} = \frac{S_A}{S_B} \times \frac{D_A}{D_B} \quad (3)$$

CHARACTERIZATION

The transmission electron microscopy (TEM) (Philips CM200 Ultra Twin) operating at 120 kV was applied to visualize the ZIF-8 particle size and shape. The ZIF-8 particles were dispersed in methanol before TEM test. One or two drops of methanol was needed to disperse ZIF-8 particles on a metal grid under a microscope. Note that the particle size distribution, XRD and N_2 adsorption tests on synthesized ZIF-8 particles were previously performed and the reported results can be found elsewhere [58].

Scanning electron microscopy (SEM) (Philips, XL 30) was used with secondary electron contrast at an acceleration voltage of 2 kV to investigate the state of aggregation of ZIF-8 particles and morphology of cross sections of synthesized MMMs.

The densities of MMMs, pure Pebax 1657 membrane and pure ZIF-8 particles were determined by a micro analytical balance (BM-22, AND) based on Archimedean principle using the following equation:

$$\rho = \frac{W_{air}}{W_{air} - W_{liq}}(\rho_{liq} - \rho_{air}) + \rho_{air} \quad (4)$$

where, W_{air} is the weight of sample in air, W_{liq} represents the measured weight of floated or submerged sample in a liquid with known density (i.e., ethanol, n-hexane, silicon oil, etc.), ρ_{air} and ρ_{liq} are, respectively, the densities of air and selected liquid. In this study, ethanol was used for density measurement and the densities were measured after permeation tests.

A differential scanning calorimeter (DSC) (PerkinElmer, Pyris 1) was used for thermal analysis. The N_2 was used as purge gas with the flowrate of 10 ml/min. Each sample was placed in an aluminum crucible with a lid and the scanning was performed three times for each sample with temperature ramp rate of 10 °C/min from –70 to 230 °C.

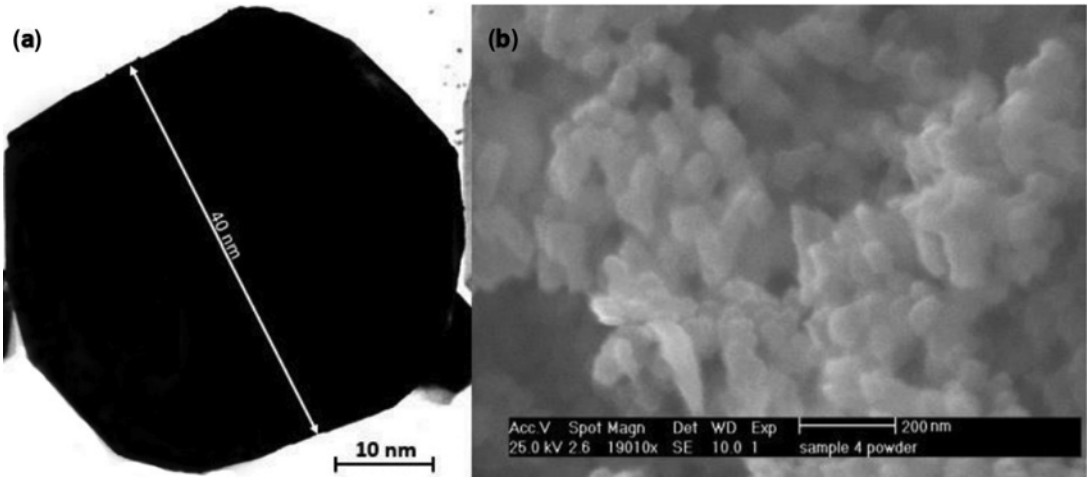

Fig. 4. (a) TEM and (b) SEM micrographs of modified ZIF-8 particles.

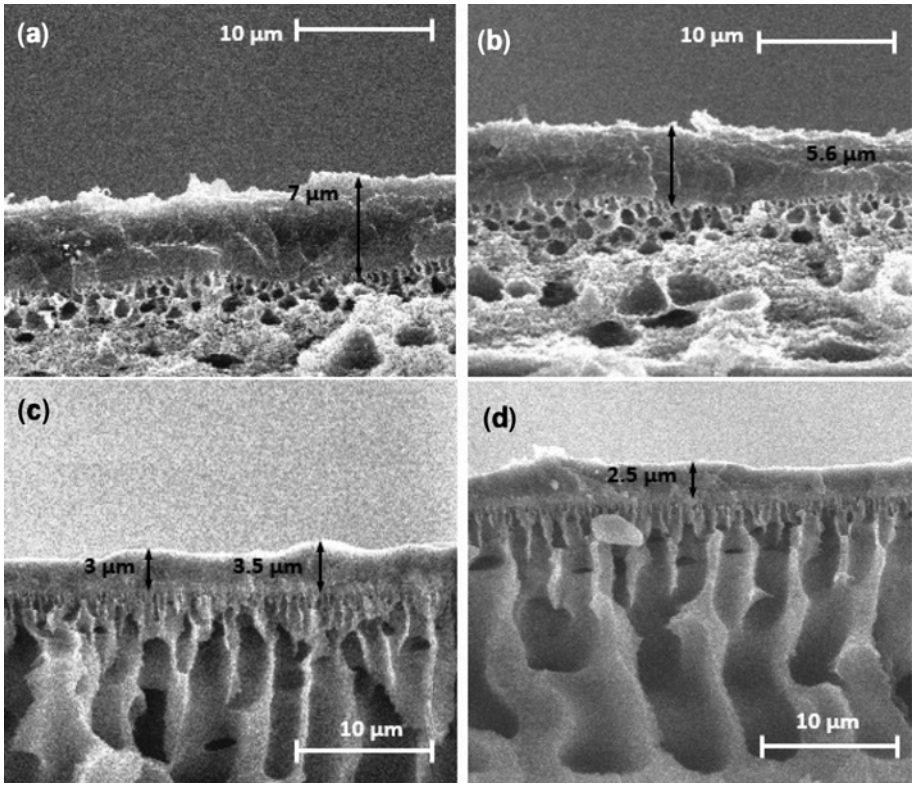

Fig. 5. SEM micrograph of cross section of ZIF-8/Pebax 1657 MMMs fabricated with 2 wt% of ZIF-8 loading with spinning speed of (a) 500 rpm (b) 1,000 rpm (c) 2,000 rpm and (d) 3,000 rpm.

RESULTS AND DISCUSSION

1. TEM and SEM Analysis

The TEM and SEM micrographs of ZIF-8 sample synthesized by molar ratio of MeIM/Zn^{2+}=32/1 at 30 °C in Pebax 1657 solution are presented in Fig. 4(a) and (b), respectively.

The rhombic shape of ZIF-8 crystal is clearly observable in Fig. 4(a). The particle size distribution of these synthesized ZIF-8 particles was reported previously by our group The ZIF-8 crystal size of about 40 nm is observable in Fig. 4(a), and it confirms the results reported by Jomekian et al. [58].

Fig. 4(b) shows the state of aggregation of ZIF-8 particles. As can be seen, ZIF-8 particles agglomerated and a huge bulk of particles was created. This occurred due to drying of the ZIF-8 after washing. The drying of a wet powder resulted in formation of agglomerated bulk; however, the bulk can be redispersed in coating solution by the aid of ultrasonic bath and vigorous agitation. Furthermore, the ZIF-8 particles have crystal sizes about 50 nm, which is in very good agreement with TEM image and by the results of particle size analysis recently reported by our group [58].

The SEM image from cross sections of MMMs which were synthesized by 2 wt% of ZIF-8 in the matrix of Pebax 1657 is presented in Fig. 5(a)-(d).

As can be seen, the selective layer is quite thinner than the porous PES support layer. This is because during the spinning of spin coater, the evaporation rate increases because of enhanced convection heat transfer resulted from movement of coated layer in air. Moreover, due to the centrifugal force, the coating solution spreads uniformly on the surface of support [62]. Accordingly, a thin and uniform coated layer has been created using spin coater for coating purpose.

From the sub-figures of Fig. 5, the angular velocity of the spin coater directly affects the spreading and the rate of evaporation of the coating solution on the support. These two factors determine the thickness of final selective layer of MMMs. It can be seen in Fig. 5(a)-(d) that the thickness of the coated layer (selective layer) decreased from 7 to 5.6 then to 3 and finally to 2.5 μm as the spinning speed of spin coater increased from 500 to 1,000 then to 2,000, and finally to 3,000 rpm, respectively. The thickness of the selective layer did not change significantly (from 3 to 2.5 μm), as the spinning speed increased from 2,000 to 3,000 rpm. This is mainly because of the dependency of thickness ratios to the square root of spinning speed ratios. Because the spinning speed ratio at high speeds (3,000 rpm/2,000 rpm) is lower than that at lower speeds, the selective layer thickness change is accordingly lower at these speeds.

The SEM images from cross sections of MMMs which were synthesized by 4 wt% of ZIF-8 in the matrix of Pebax 1657 are presented in Fig. 6(a)-(d).

From the subfigures of Fig. 6, as the spinning speed increases a smoother selective surface is created. The thickness of selective

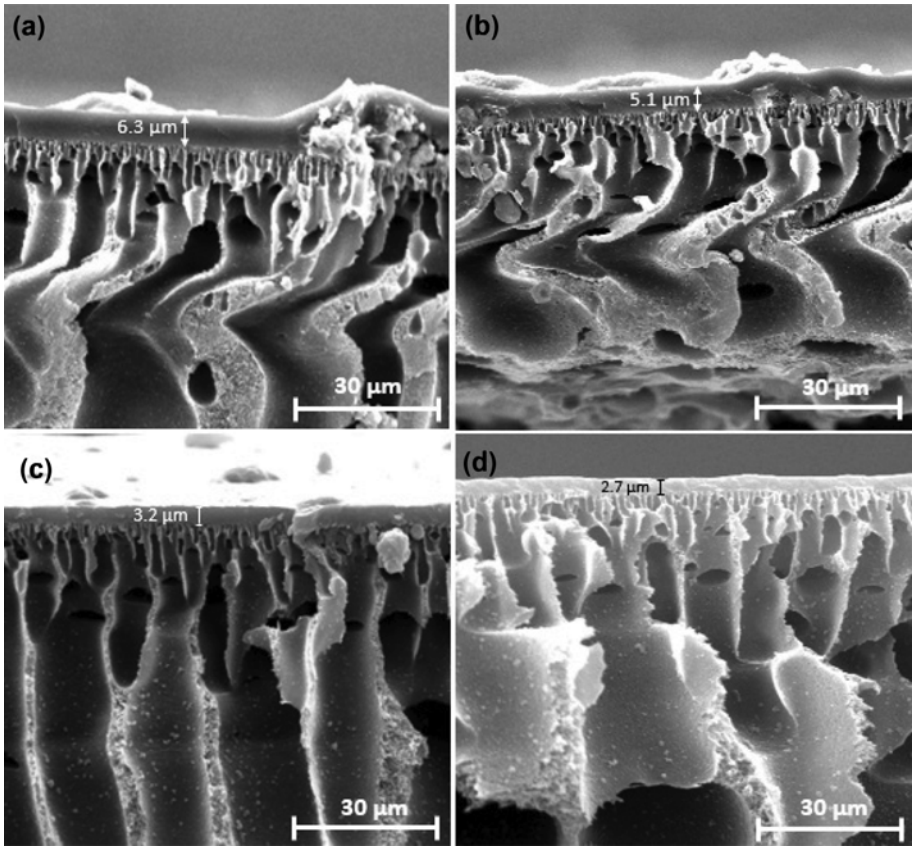

Fig. 6. SEM micrograph of cross section of ZIF-8/Pebax 1657 MMMs fabricated with 4 wt% of ZIF-8 loading with spinning speed of (a) 500 rpm (b) 1,000 rpm (c) 2,000 rpm and (d) 3,000 rpm.

layer changed from 6.3 to 5.1 then to 3.2 and finally to 2.7 μm as the spinning speed of spin coater increased from 500 to 1,000 the to 2,000 and finally to 3,000 rpm, respectively. The same trend and order of magnitude of change in thickness of selective layer that had been observed for samples synthesized by lower loadings of ZIF-8 is also observable for the samples synthesized by higher loading of ZIF-8. The thickness of the coated layer is less than 6.3 μm for all prepared MMM samples, which demonstrates that the spin

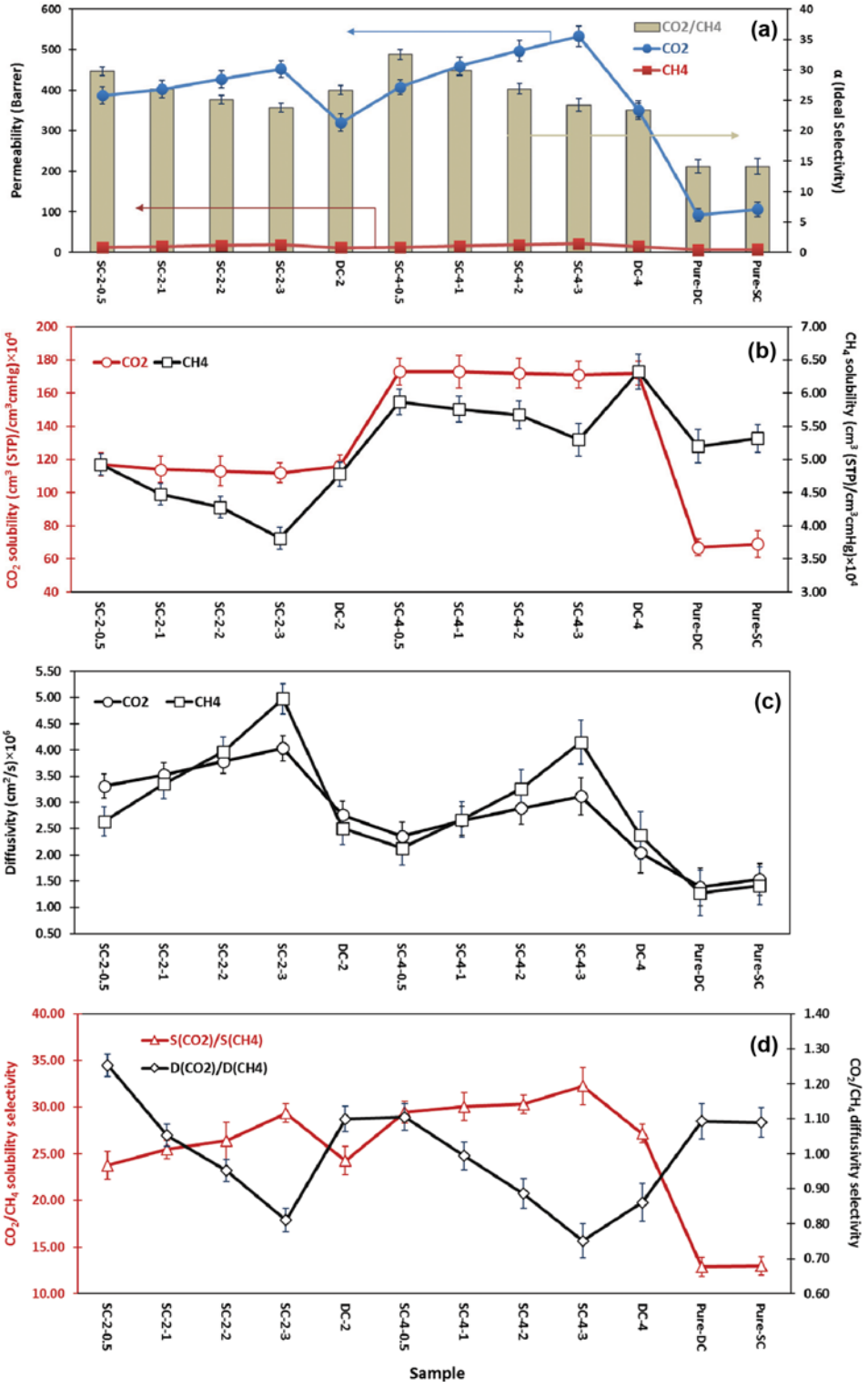

Fig. 7. The (a) permeability of CO_2 and CH_4 and the ideal selectivity of CO_2/CH_4 (b) solubility of CO_2 and CH_4 (c) diffusivity of CO_2 and CH_4 and (d) CO_2/CH_4 solubility selectivity and diffusivity selectivity of synthesized membranes determined in pure gas tests at feed pressure of 5 bar.

coating led to the formation of a thin selective layer in all synthesized MMMs.

2. Gas Permeation Measurements

2-1. The Effect of Synthesis Parameters

2-1-1. Pure Gas Test (Ideal Performance)

Fig. 7(a) illustrates the effect of coating method, spinning speed and loading of ZIF-8 in the matrix of Pebax 1657 on permeabilities of CO_2 and CH_4 and on ideal selectivity of CO_2/CH_4. All of permeation tests were performed at constant feed pressure of 5 bar.

Form this figure, all of the synthesized MMMs show superior performance compared to pure Pebax 1657. Fig. 7(a) also shows that as the spinning speed of spin coater increases, the permeabilities of both CO_2 and CH_4 increase. This is mainly due to the decrease of thickness of selective layer with spinning speed. Although at equilibrium the amount of CO_2 that is absorbed per unit volume of membrane is the same for both thick and thin membranes, as can be seen in Fig. 7(b), the thinner selective layer is more vulnerable to plasticization and disruption of polymer chains due to the high sorption of CO_2.

Fig. 7(b) presents the solubility coefficients of CO_2 (S_{CO_2}) and CH_4 (S_{CH_4}) obtained in gas sorption tests at 5 bar. S_{CO_2} is almost constant for MMMs having the same loading of ZIF-8 in their matrix. This demonstrates that these MMMs reached almost the same equilibrium CO_2 sorption capacity at 5 bar. However, for the case of S_{CH_4}, a decreasing trend is observed as the spinning speed of coating increases. This is most probably because there is a weak tendency in both Pebax 1657 and ZIF-8 for sorption of CH_4. The weak sorption of this gas is very dependent on the thickness of MMMs. As the membrane becomes thinner, the void volume fraction in MMMs increases. The void volume in MMMs does not have CH_4 sorption ability; therefore, the solubility of CH_4 in thinner MMMs shows lower value compared with thicker MMMs.

The high sorption capacity for CO_2 which is observable in Fig. 7(b) is mainly because the EO groups in Pebax 1657 matrix exhibit strong affinity for CO_2; thus, the solubility of this gas in PEO is high. More importantly, the ultra-porous ZIF-8 particles with modified pore structures have also very strong intrinsic affinity for CO_2 adsorption. This is the reason for the significantly higher solubility and therefore permeability of CO_2 in ZIF-8/Pebax 1657 MMMs compared to CH_4, which can be clearly observed in Fig. 7(a).

Although the CO_2 permeability significantly increases with reduction of the selective layer thickness, the permeability of CH_4 is more affected by that reduction (Fig. 7(a)). This demonstrates that in MMMs with thinner selective layer the increased polymer chain mobility, which probably resulted from plasticization due to the extra sorption of CO_2, is the main reason of partial separation disability of membranes. The results of CO_2/CH_4 ideal selectivity approve this hypothesis very well.

Also in Fig. 7(a), with increase in ZIF-8 particles loading in the matrix of Pebax 1657, the permeabilities of both CO_2 and CH_4 increase. However, as the loading of ZIF-8 increases, the change of CO_2 permeability becomes more recognizable than the change of CH_4 permeability. One may think this is due to the enhanced diffusivity of CO_2 through pores of ZIF-8 because of the smaller kinetic diameter of CO_2 molecules than CH_4 molecules; however, the results of Fig. 7(c) lead one to reject this hypothesis. As can be seen in Fig. 7(c), the diffusivities of CO_2 and CH_4 are of the same order of magnitude; therefore, these gases diffuse similarly through pores of ZIF-8, which is a logical behavior considering the modified pore size of ZIF-8 particles. The reason for significantly higher permeability of CO_2 is related to the significantly higher sorption of this gas in the pores of ZIF-8, which can be clearly seen in Fig. 7(b).

Fig. 7(d) presents the solubility selectivities and diffusivity selectivities of MMMs and Pebax 1657 pure membranes. As is clear, the solubility selectivity of MMMs having the same ZIF-8 loading exhibits an increasing trend with increase of the spinning speed of coating process. This is due to the decreased sorption capacity of ZIF-8 for MMMs having thinner selective layer as was explained.

From this figure it can be easily deduced that the selective separation of CO_2 from CH_4 is mainly due to high solubility selectivity of MMMs. There is not an effective diffusivity selectivity involvement in CO_2/CH_4 ideal selectivity. Even a reverse CO_2/CH_4 diffusivity selectivity is observed for thin MMMs. The reason is related to the increase in size of ZIF-8 pores which weaken its molecular sieving ability; hence both CO_2 and CH_4 molecules with different kinetic dimeters can similarly pass through pores of ZIF-8 leading to deterioration of diffusivity selectivity of MMMs.

Note that the MMMs synthesized by dip coating method have significantly lower CO_2 permeability compared to MMMs synthesized by spin coating method (Fig. 7(a)). However, the CO_2/CH_4 selectivity in these MMMs is comparable to the MMMs synthesized by high spinning speed. This is because dip coating often results in the formation of relatively thicker selective layer compared to spin coating with high spinning speed. Generally, with thicker selective layer of membrane the probability of formation of defect minimizes; therefore, it was expected that the CO_2/CH_4 ideal selectivity of synthesized MMMs by dip coating would be higher compared to MMMs synthesized by spin coating. However, the formation of uniform and defect-free selective layer of Pebax 1657 using dip coating is difficult and a rugged surface forms as can be seen in Fig. 8.

This non-uniform surface demonstrates that dip coating with this thickness cannot completely cover the roughness of the PES support, probably due to the penetration of coating solution into

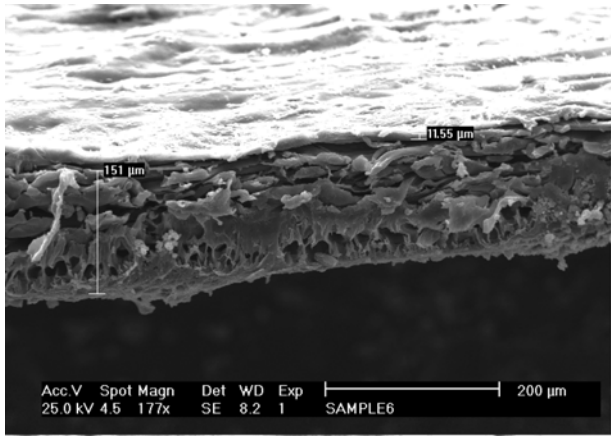

Fig. 8. The cross-section and surface of a ZIF-8/Pebax 1657 MMM synthesized by dip coating method.

the macropores of support, which does not happen in spin coating due to the rapid rate of solvent evaporation. This incomplete coating using dip coating method is the main reason for lower CO_2/CH_4 selectivity even with thicker selective layer (~11.55 μm) of dip coated MMMs compared to spin coated MMMs.

2-1-2. FFV and φ_V Calculations

To investigate the effect of ZIF-8 porous particles on free volume of Pebax 1657 in the resulting MMMs, the fractional free volume (FFV) of MMMs and Pebax 1657 pure membranes was estimated using measured densities of MMMs, pure Pebax 1657 membranes and pure ZIF-8 particles. For pure Pebax 1657 membranes the FFVs were calculated by the following equation [63]:

$$FFV = \frac{V_{Pebax} - V_{0,\,Pebax}}{V_{Pebax}} = \frac{M_{Pebax}/\rho_{Pebax} - 1.3V_{W,\,Pebax}}{M_{Pebax}/\rho_{Pebax}} \quad (5)$$

where V_{Pebax} is total molar volume of Pebax 1657 (cm^3/mol), $V_{0,\,Pebax}$ is volume occupied by polymer chains (cm^3/mol), M_{Pebax} is the molar weight of a monomer of Pebax 1657 (g/mol), ρ_{Pebax} is the density of pure Pebax 1657 membrane (g/cm^3), and $V_{W,\,Pebax}$ is the van der Waals volume of Pebax 1657 (cm^3/mol). The van der Waals volume in this study was determined by Bondi's group contribution method by taking into account just PEO and PA6 segments in the structure of Pebax 1657. The value of V_W=95.09 cm^3/mol was obtained for Pebax 1657 using Bondi's group contribution method [64].

For the case of MMMs the contribution of ZIF-8 particles in Pebax 1657 matrix must be taken into account; therefore, it is required to determine the volume fraction of ZIF-8 in MMMs. The following equation can be helpful for this purpose [65]:

$$\varphi_{ZIF} = \frac{\omega_{ZIF}/\rho_{ZIF}}{\omega_{ZIF}/\rho_{ZIF} + (1-\omega_{ZIF})/\rho_{Pebax}} \quad (6)$$

where φ_{ZIF} is the volume fraction of ZIF-8 in MMM, ω_{ZIF} is the mass fraction of ZIF-8 in MMM and ρ_{ZIF} is the density of ZIF-8 particles.

Using φ_{ZIF} and ρ_{ZIF}, the FFVs for MMMs can be calculated by the following equation:

$$FFV = \frac{v_{MMM} - [(1.3V_{W,\,Pebax}/M_{Pebax})(1-\varphi_{ZIF}) + (\varphi_{ZIF}/\rho_{ZIF})]}{v_{MMM}} \quad (7)$$

where v_{MMM} is the specific volume of MMM (cm^3/g), which is the inverse of density of MMM. The void volume fraction of MMMs (φ_V), which indicates the percentage of increase in void volume as a result of alteration in polymer chain packing after permeation tests, has been also calculated by:

$$\varphi_V = \frac{\rho_T - \rho_E}{\rho_E} \quad (8)$$

where ρ_E is the experimentally measured density of MMM and ρ_T is the theoretical density of MMM which is calculated by:

$$\rho_T = \frac{1}{\omega_{ZIF}/\rho_{ZIF} + (1-\omega_{ZIF})/\rho_{Pebax}} \quad (9)$$

The calculated values of FFVs for pure membranes and MMMs along with φ_{ZIF} and φ_V for MMMs are presented in Table 2. The values of experimentally measured densities of all samples are also shown in this table.

As can be seen, there is a decreasing trend for measured densities of MMMs with the increase in speed of spin coating for synthesis of MMMs. This observation is mainly due to the occurrence of plasticization phenomenon. As observed in DSC results, MMMs with thinner selective layer plasticize more severely than other MMMs. The plasticization interrupts the chain packing of Pebax 1657; therefore, the free volume in polymers increases, and this increase leads to an increase in total volume of a MMM with a constant mass, leading to decrease in MMM density.

Table 2. The measured and calculated structural properties of synthesized samples

Samples	φ_{ZIF}	ρ (g/cm^3)	FFV	φ_V
ZIF-8 particles	-	1.393	-	-
Pure SC	0	1.13	0.110	0
Pure DC		1.14	0.102	0
SC-2-0.5	0.0164	1.12	0.122	0.013
SC-2-1		1.11	0.128	0.022
SC-2-2		1.09	0.144	0.040
SC-2-3		1.05	0.176	0.080
DC-2		1.10	0.137	0.040
SC-4-0.5	0.033	1.10	0.137	0.035
SC-4-1		1.08	0.152	0.055
SC-4-2		1.04	0.212	0.095
SC-4-3		0.98	0.231	0.162
DC-4		1.05	0.176	0.093

The other factor that affects the densities of MMMs is the incorporation of ZIF-8 porous particles into the matrix of Pebax 1657. ZIF-8 particles in Pebax 1657 matrix increases the free volume of the resulting MMMs, with interruption of Pebax 1657 chain packing around these particles leading to the same effect that plasticization had on these MMMs.

The calculated values of FFVs increase as the densities of MMMs decrease; this increase was more distinguishable for MMMs synthesized by higher loadings of ZIF-8 (4 wt%). This is because, in addition to plasticization effect, higher loading of ZIF-8 in the matrix of Pebax 1657 leads to more interruption in chain packing of Pebax 1657 and consequently creation of higher free volume and FFV in MMMs [66]. Moreover, in MMMs synthesized by higher loadings of ZIF-8, higher values of φ_V were observed. The reasons for this observation are twofold. One is related to the fact that as ZIF-8 particles have been introduced into the Pebax 1657 matrix, due to the partial incompatibility at particle-polymer interface, microvoids have been created. The creation of interfacial microviods is dependent on particle-polymer interfacial area; therefore, as the loading of ZIF-8 increases in MMMs, because of the increase in particle-polymer interfacial area, φ_V increases. More importantly, the enhanced porosity and increased pore size of ZIF-8 particles directly affects the void volume of the whole MMMs, so the void volume fraction (φ_V) of MMMs with higher loadings of ZIF-8 is significantly higher compared to MMMs prepared with lower loadings of ZIF-8.

The increases in FFV and φ_V for MMMs synthesized with higher spinning speeds are two main reasons for increase in permeability

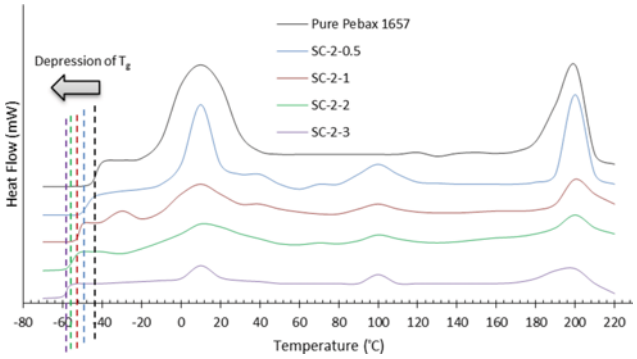

Fig. 9. DSC therograms of synthesized ZIF-8/Pebax 1657 MMMs in comparison with Pebax 1657 pure membrane.

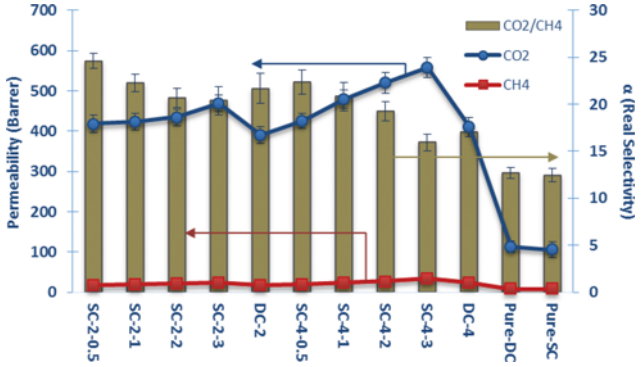

Fig. 10. The permeability of CO_2 and CH_4 and the real selectivity of CO_2/CH_4 of synthesized membranes determined in mixed gas tests at feed pressure of 5 bar.

of gases through these MMMs. Moreover, higher values of φ_V for these MMMs demonstrates the partial deterioration of selective performance of MMMs; therefore, for these thin MMMs lower CO_2/CH_4 selectivities have been observed.

2-1-3. DSC Analysis

To investigate the occurrence of plasticization phenomenon during gas permeation tests the DSC test was conducted. The samples selected for DSC analysis were all exposed to CO_2 and CH_4 for 12 hours during the permeation tests prior to DSC analysis in the exact similar conditions of pressure (5 bar) and temperature (30 °C). The results of DSC of synthesized MMMs and a pure Pebax 1657 membrane are presented in Fig. 9.

As can be seen, for all membrane samples a noticeable rise in heat flow in the range of −60 °C to −40 °C can be distinguished. This rise is due to the increase in heat capacity of polymer because of transition of polymer from glassy to rubbery state. The mean temperature where this rise occurs is called the glass transition temperature (T_g). It can be seen that the T_g of MMMs decreased compared to T_g of pure Pebax 1657 membrane. This decrease in T_g was more significant for MMMs synthesized with higher speeds of spin coater. As one of the subsequences of plasticization is known to be a minor decrease in T_g of polymer [67], it can be deduced that the Pebax 1657 was plasticized in MMMs during the CO_2 and CH_4 permeation evaluation. This phenomenon was more influential on the chain mobility of MMMs synthesized with higher speeds of spin coater, which is directly related to the permeation behavior of these membranes.

Furthermore, for pure Pebax 1657 membrane two distinctive peaks can be observed at about 10 °C and 200 °C, which are related to the fusion of crystalline fractions of PEO and PA6 segments of Pebax 1657, respectively. As the temperature increases, initially PEO at 12 °C and then PA6 at 202 °C start to melt. Therefore, the need of energy for temperature change at melting points increases, which results in observation of the peaks.

As can be seen, the relative height of fusion peaks decreases as the thickness of the selective layer increases. This observation demonstrates that the phase change of PEO and PA6 segments partially occurred during permeation test and before DCS analysis. This phase change can be related to the plasticization of Pebax 1657 segments during the permeation tests. Some small peaks are also observable in DSC curves of synthesized MMMs in about 100 °C, which is probably due to the evaporation of adsorbed moistures in ZIF-8 pores during heating.

2-1-4. Mixed Gas Test (Real Performance)

The gas mixture of 10 vol% CO_2 and 90 vol% CH_4 was prepared by means of gas permeation setup for mixed gas permeation tests. Fig. 10 illustrates the effect of coating method, spinning speed and loading of ZIF-8 in the matrix of Pebax 1657 on permeabilities of CO_2 and CH_4 and on real selectivity of CO_2/CH_4.

In this figure, the same trends of changes in permeabilities and selectivities, which were observed in pure gas tests, are also observed in mixed gas tests. However, the CO_2/CH_4 separation performances of all MMMs were enhanced in terms of CO_2 permeability and deteriorated in terms of CO_2/CH_4 selectivity compared to the pure gas test results. The reduction in CO_2/CH_4 real selectivity values in mixed gas tests compared to pure gas tests is mainly due to the partial plasticization of PEO segments of Pebax 1657 because of the exposure to CO_2 for a relatively long period of time (10-12 h) of permeation tests. Similar trends of changes in CH_4 permeability are also observed in previous works on MMMs.

The reason for increase in permeability of CO_2 in mixed gas tests compared to pure gas tests, which is rarely reported in the literature, is related to the increase in solubility of CO_2 in PEO segments at presence of CH_4. Similar behavior was reported by Freeman group [68] in mixed gas test for CO_2/C_2H_6 separation by cross-linked PEO copolymer with the exact feed composition used in this study. It can be said that the diffusivity of CO_2 in Pebax 1657 matrix did not have significant effect on increase of permeability of CO_2 in mixed gas state. Plasticization of chain packing of the Pebax 1657 membrane is known to be another reason for increased CO_2 permeability in mixed gas tests compared to pure gas test, as it was proved by the Chung group [69] in a study on CO_2/H_2 separation by POSS/Pebax 1657 MMMs.

2-2. The Effect of Feed Pressure

The effect of different total pressures of mixed feed (10 vol% CO_2, 90 vol% CH_4) on the CO_2 permeability of synthesized MMMs is presented in Fig. 11.

From this figure, it is clear that with increase in feed pressure, the CO_2 permeabilities of all synthesized ZIF-8/Pebax 1657 MMMs increase. This is because the PEO segments of Pebax 1657 are mainly responsible for the overall separation performance of Pebax 1657.

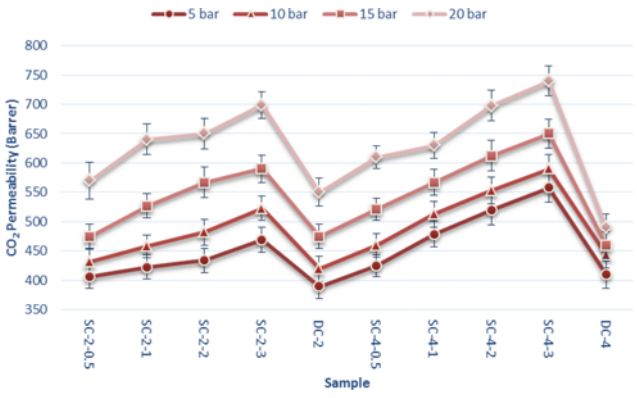

Fig. 11. The effect of mixed gas feed pressure on CO_2 permeability of all synthesized ZIF-8/Pebax 1657 MMMs.

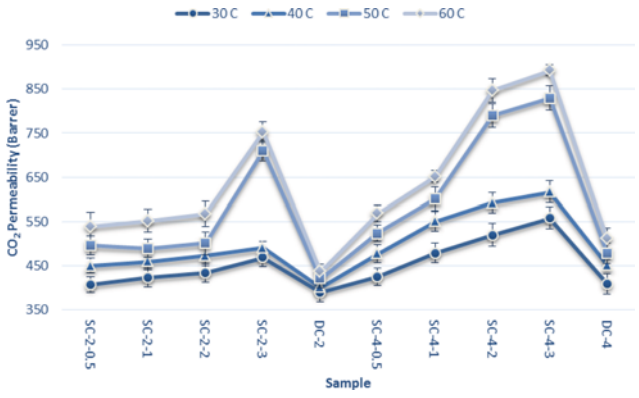

Fig. 13. The effect of testing temperature on CO_2 permeability of all synthesized ZIF-8/Pebax 1657 MMMs.

The PEO is in rubbery state at ambient temperature ($T_g \approx -50$ to -57 °C) and for a rubbery polymer the role of diffusivity of gases in the overall permeability is often insignificant compared to the solubility role, as it was previously explained. As the feed pressure increases, the diffusion of gases through the membranes become more difficult because of the compactness of polymer chains and consequently the decrease of the FFVs of membranes in higher pressures [70,71]. However, this does not have significant impact on the overall permeability because PEO is a strong absorber of CO_2, thus the solubility of CO_2 in this polymer is very high. Moreover, the solubility of gases in polymers has a direct relationship with the feed pressure. Therefore, as the feed pressure increases, the solubility of CO_2 in all prepared MMMs increases. Because the permeability of CO_2 in Pebax 1657 is mainly affected by its solubility rather than its diffusivity, the permeability of CO_2 in all MMMs increases with pressure. On the other hand, ZIF-8 with enhanced porosity also has strong affinity for CO_2. The structure of ZIF-8 is rigid and does not compact due to the applied pressure; therefore, both diffusivity and sorption in ZIF-8 pores increase with increase of applied feed pressure.

The CO_2/CH_4 selectivities in different pressures, which is presented in Fig. 12, demonstrates that with increase in feed pressure the selectivity decreases. This decrease is significant in the test conducted at 20 bars. This is because at higher pressures the effect

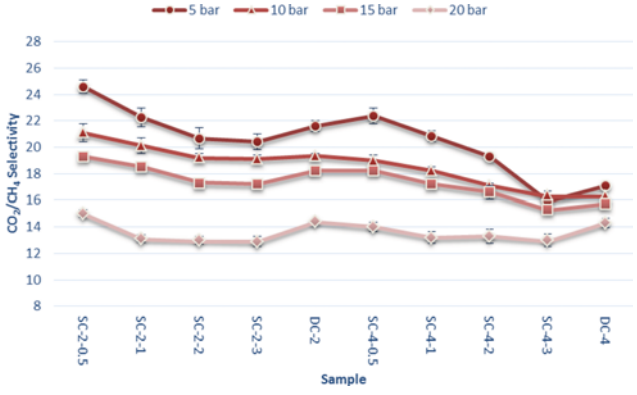

Fig. 12. The effect of mixed gas feed pressure on CO_2/CH_4 selectivity of all synthesized ZIF-8/Pebax 1657 MMMs.

of the particles-polymer interfacial voids or incompatibilities intensifies. At higher pressures, gas molecules favor voids instead of the matrix of Pebax of ZIF-8 pores to pass through. The results of selectivities show that the CO_2 high permeabilities are not only due to high affinity of Pebax matrix and ZIF-8 particles for this gas. The interfacial voids created in higher pressures have also a role in high CO_2 permeation results. Moreover, the plasticization effect is directly related to the applied feed pressures; therefore, at higher pressure it is expected that the performance of synthesized ZIF-8 Pebax 1657 MMMs deteriorates to some extent.

2-3. The Effect of Temperature

Mixed gas permeation tests were also performed at different temperatures (30, 40, 50 and 60 °C) at 5 bar. Fig. 13 depicts the effect of testing temperatures on the CO_2 permeabilities of all synthesized MMMs.

From this figure, one can deduce that the testing temperature has increasing effect on CO_2 permeability for all synthesized MMMs. The reason for this observation is partly due to the increase in diffusivity because of enhanced flexibility of PA6 and PEO chains with temperature [59]. Although the diffusivity has a minor effect on permeability at ambient temperature, the results from previous works show that the diffusivity of CO_2 in Pebax 1657 remarkably increased with temperature that strongly affected the permeability according to solution-diffusion theory [36,59]. Apart from that, as the chains of Pebax 1657 become more flexible, the disrupted chains at particle-polymer interface also become more flexible; therefore, the effect of rigidification of the particle-polymer interface weakened. In a rigidified interface, the selectivity is higher but the permeability is lower compared to those in defect free interface [72-75]. Therefore, at higher temperatures because of more flexible particle-polymer interface, a higher permeability and lower selectivity are expected for MMMs.

In addition, the solubility of CO_2 in Pebax 1657 decreases with temperature because the enthalpy of sorption of CO_2 in Pebax 1657 is negative [21,59]. Therefore, the increase in the overall CO_2 permeability is not due to the solubility enhancement. Although the solubility of CO_2 in Pebax 1657 decreases with temperature, it seems that this decrease in solubility is not as large as the increase in diffusivity. Therefore, the overall permeability increases with temperature.

It is also evident in Fig. 13 that the spinning speed had signifi-

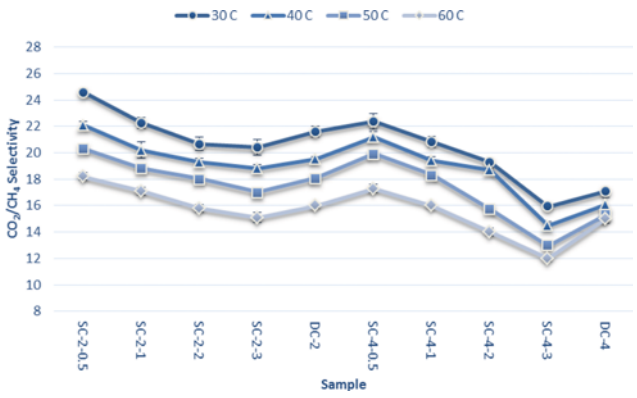

Fig. 14. The effect of testing temperature on CO_2/CH_4 selectivity of all synthesized ZIF-8/Pebax 1657 MMMs.

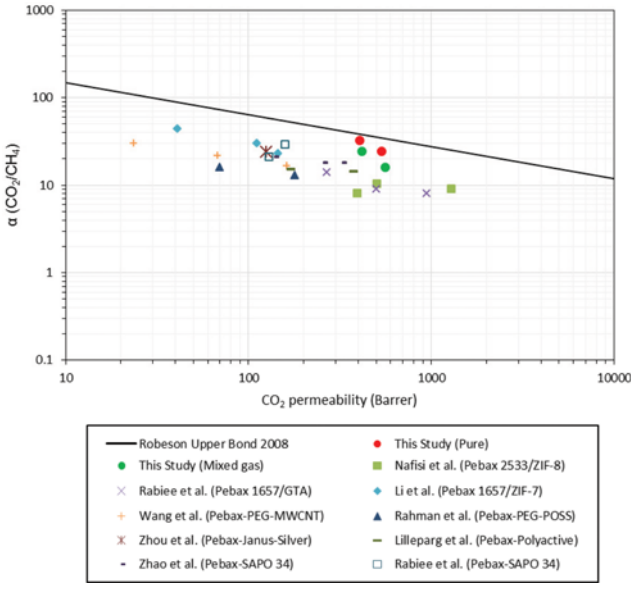

Fig. 15. Comparison of CO_2/CH_4 separation performance of MMMs synthesized in this study by that of recent Pebax based membranes reported in literature.

cant effect on CO_2 permeability in higher temperatures. MMMs synthesized with high spinning speed (3,000 rpm) of spin coater have unusually highest CO_2 permeability in 50 °C and 60 °C. As the selective layer becomes thinner, the role of ZIF-8 particles in separation becomes more important. Therefore, an interfacial defect can be more serious in MMMs with thinner selective layer. These interfacial defects, as explained before, have increasing effects at higher temperatures on permeability. Moreover, the plasticization effect at higher temperatures is more serious, especially for MMMs with thinner selective layer because the flexibility of polymer chains increases with temperature, and this flexible structure is more vulnerable to high CO_2 sorption. Therefore, at higher temperatures enhanced CO_2 permeability can be observed, which is mainly due to the structural changes. This hypothesis is confirmed by the results presented in Fig. 14.

As can be seen in Fig. 14, the synthesized MMMs with higher spinning speed (thinner) at higher temperatures suffer from the low CO_2/CH_4 selectivity. The is because the increased mobility of the Pebax 1657 chains in higher temperatures leads to partial loss of selective separation ability of Pebax matrix. On the other hand, the rigidified particle-polymer interface has more effect on selectivity at lower temperatures in MMMs synthesized by higher loading of ZIF-8. This leads to higher CO_2/CH_4 selectivity at lower temperatures, as explained previously.

Although the CO_2 permeabilities of (SC-2-3), (SC-4-2) and (SC-4-3) were remarkably higher than that of other synthesized MMMs, the drop in their CO_2/CH_4 selectivity is not as large as the increase in their permeability. It implicitly demonstrates that the particle-polymer interface was synthesized without significant voids; otherwise the selectivity must have dropped drastically for the mentioned MMM samples.

The CO_2/CH_4 separation performance of two synthesized ZIF-8/Pebax 1657 MMMs having maximum CO_2 permeability (SC-4-3) and maximum CO_2/CH_4 selectivity (SC-4-0.5) in both pure and mixed gas tests is shown on Robeson upper bond graph 2008 (Fig. 15). The permeability and selectivity of both presented membranes were evaluated at pressure of 5 bar and temperature of 30 °C. The performance of other synthesized samples, which have not been shown here for the sake of brevity, is around the presented points. As can be seen, the synthesized samples in this study almost reached the upper bound and have superior performance compared to the most of the Pebax based membranes synthesized in other works.

CONCLUSION

Multilayer ZIF-8/Pebax 1657 MMMs were synthesized with modified ZIF-8 particles using a manually made spin coater. The overall results showed that the spinning speed of the spin coater had a significant effect on the performance of synthesized MMMs. As the spinning speed increased, the permeabilities of CO_2 and CH_4 increased; however, a decline in ideal and real selectivity of CO_2/CH_4 was also observed. Compared to dip coating method, the MMMs synthesized by spin coating at lower spinning speeds (500 and 1,000 rpm) had better separation performance in both pure and mixed gas tests. The plasticization was recognized as the main reason for inferior separation performance of MMMs with thinner selective layer.

Applying higher mixed feed pressures and permeation tests temperatures resulted in increase in CO_2 permeability and decrease in CO_2/CH_4 selectivity for almost all investigated MMMs. The plasticization affected the performance of MMMs more in higher feed pressures.

The CO_2 and CH_4 permeabilities of synthesized MMM with thinnest selective layer were remarkably high, while its CO_2/CH_4 selectivity was comparable to that of other MMMs in temperature of 60 °C.

The synthesized modified ZIF-8/Pebax 1657 MMMs showed superior performances in pure gas tests and competitive performance in mixed gas tests for CO_2/CH_4 separation compared to the state of the art Pebax based membranes synthesized and reported in literature.

ACKNOWLEDGEMENT

The National Iranian Gas Company (NIGC) is gratefully acknowl-

edged for providing financial support of this work (Grant No: 193075).

NOMENCLATURE

P_i : permeability of gas component i [barrer]
Q_i : volumetric flowrate of component i [cm^3]
l : membrane selective layer thickness [cm]
A : effective surface area of membrane [cm^2]
p_{fi} : partial pressure of component i at feed side [cmHg]
p_{pi} : partial pressure of component i at permeate side [cmHg]
$\alpha_{A/B}$: ideal selectivity of gas A to gas B
D_i : diffusivity of component i [cm^2/s]
S_i : solubility of component i [cm^3 (STP)/cm^3·cmHg]
ρ_{air} : the density of air [g/cm^3]
ρ_{liq} : the density of determinant liquid [g/cm^3]
W_{air} : the weight of sample in air [g]
W_{liq} : the weight of sample in determinant liquid [g]
FFV : fractional free volume
V_{Pebax} : total molar volume of Pebax 1657 [cm^3/mol]
$V_{0, Pebax}$: volume occupied by polymer chains [cm^3/mol]
M_{Pebax} : molar weight of a monomer of Pebax 1657 [g/mol]
ρ_{Pebax} : density of pure Pebax 1657 membrane [g/cm^3]
$V_{W, Pebax}$: Van der Waals volume of Pebax 1657 [cm^3/mol]
φ_{ZIF} : volume fraction of ZIF-8 in mixed matrix membrane
ρ_{ZIF} : density of ZIF-8 particles [g/cm^3]
ω_{ZIF} : mass fraction of ZIF-8 in mixed matrix membrane
v_{MMM} : specific volume of mixed matrix membrane [cm^3/g]
φ_V : void volume fraction
ρ_T : theoretical density of mixed matrix membrane [g/cm^3]
ρ_E : experimental density of mixed matrix membrane [g/cm^3]

REFERENCES

1. A. Jomekian, R. M. Behbahani, T. Mohammadi and A. Kargari, *J. Nat. Gas. Sci. Eng.*, **31**, 562 (2016).
2. E. Ebrahimzadeh, J. Matagi, F. Fazlollahi and L. L. Baxter, *Appl. Therm. Eng.*, **96**, 39 (2016).
3. F. Fazlollahi, A. Bown, E. Ebrahimzadeh and L. L. Baxter, *Energy*, **90, Part 1**, 244 (2015).
4. F. Fazlollahi, A. Bown, E. Ebrahimzadeh and L. L. Baxter, *Energy*, **103**, 369 (2016).
5. E. Ebrahimzadeh and L. L. Baxter, *Appl. Therm. Eng.*, **102**, 785 (2016).
6. M. Binns, S.-Y. Oh, D.-H. Kwak and J.-K. Kim, *Korean J. Chem. Eng.*, **32**, 383 (2015).
7. C. Chen, J. Kim and W.-S. Ahn, *Korean J. Chem. Eng.*, **31**, 1919 (2014).
8. H. Lin, E. VanWagner, R. Raharjo, B. D. Freeman and I. Roman, *Adv. Mater.*, **18**, 39 (2006).
9. M. Rezakazemi, A. Ebadi Amooghin, M. M. Montazer-Rahmati, A. F. Ismail and T. Matsuura, *Prog. Polym. Sci.*, **39**, 817 (2014).
10. L. M. Robeson, *J. Membr. Sci.*, **320**, 390 (2008).
11. V. M. Aceituno Melgar, J. Kim and M. R. Othman, *J. Ind. Eng. Chem.*, **28**, 1 (2015).
12. D. Bastani, N. Esmaeili and M. Asadollahi, *J. Ind. Eng. Chem.*, **19**, 375 (2013).
13. S. R. Venna and M. A. Carreon, *Chem. Eng. Sci.*, **124**, 3 (2015).
14. M. H. Nematollahi, A. H. S. Dehaghani and R. Abedini, *Korean J. Chem. Eng.*, **33**, 657 (2016).
15. J. Lillepärg, P. Georgopanos and S. Shishatskiy, *J. Membr. Sci.*, **467**, 269 (2014).
16. H. Yang, Z. Xu, M. Fan, R. Gupta, R. B. Slimane, A. E. Bland and I. Wright, *J. Environ. Sci.*, **20**, 14 (2008).
17. M. Buonomenna, W. Yave and G. Golemme, *RSC Adv.*, **2**, 10745 (2012).
18. R. Hilke, N. Pradeep, A. R. Behzad, S. P. Nunes and K.-V. Peinemann, *J. Membr. Sci.*, **472**, 39 (2014).
19. E. Ahmadpour, A. A. Shamsabadi, R. M. Behbahani, M. Aghajani and A. Kargari, *J. Nat. Gas Sci. Eng.*, **21**, 518 (2014).
20. M. A. Ardestani, A. Babaluo, M. Peyravi, M. R. Aghjeh and E. Jannatdoost, *Desalination*, **250**, 1140 (2010).
21. J. C. Chen, X. Feng and A. Penlidis, *Sep. Sci. Technol.*, **39**, 149 (2005).
22. Y. Chen, B. Wang, L. Zhao, P. Dutta and W. S. Winston Ho, *J. Membr. Sci.*, **495**, 415 (2015).
23. E. Esposito, G. Clarizia, P. Bernardo, J. C. Jansen, Z. Sedláková, P. Izák, S. Curcio, B. d. Cindio and F. Tasselli, *Chem. Eng. Process. Process Intensif.*, **94**, 53 (2015).
24. S. Feng, J. Ren, H. Li, K. Hua, X. Li and M. Deng, *J. Energ. Chem.*, **22**, 837 (2013).
25. S. Feng, J. Ren, Z. Li, H. Li, K. Hua, X. Li and M. Deng, *Int. J. Greenhouse Gas Control*, **19**, 41 (2013).
26. A. Ghadimi, T. Mohammadi and N. Kasiri, *Int. J. Hydrogen Energy*, **40**, 9723 (2015).
27. T. Li, Y. Pan, K.-V. Peinemann and Z. Lai, *J. Membr. Sci.*, **425-426**, 235 (2013).
28. R. S. Murali, K. P. Kumar, A. Ismail and S. Sridhar, *Micropor. Mesopor. Mater.*, **197**, 291 (2014).
29. R. S. Murali, S. Sridhar, T. Sankarshana and Y. Ravikumar, *Ind. Eng. Chem. Res.*, **49**, 6530 (2010).
30. V. Nafisi and M.-B. Hägg, *J. Membr. Sci.*, **459**, 244 (2014).
31. J. Potreck, K. Nijmeijer, T. Kosinski and M. Wessling, *J. Membr. Sci.*, **338**, 11 (2009).
32. H. Rabiee, S. Meshkat Alsadat, M. Soltanieh, S. A. Mousavi and A. Ghadimi, *J. Ind. Eng. Chem.*, **27**, 223 (2015).
33. H. Rabiee, M. Soltanieh, S. A. Mousavi and A. Ghadimi, *J. Membr. Sci.*, **469**, 43 (2014).
34. M. M. Rahman, V. Filiz, S. Shishatskiy, C. Abetz, S. Neumann, S. Bolmer, M. M. Khan and V. Abetz, *J. Membr. Sci.*, **437**, 286 (2013).
35. M. M. Rahman, S. Shishatskiy, C. Abetz, P. Georgopanos, S. Neumann, M. M. Khan, V. Filiz and V. Abetz, *J. Membr. Sci.*, **469**, 344 (2014).
36. J. H. Kim and Y. M. Lee, *J. Membr. Sci.*, **193**, 209 (2001).
37. R. Surya Murali, A. F. Ismail, M. A. Rahman and S. Sridhar, *Sep. Purif. Technol.*, **129**, 1 (2014).
38. J. Cravillon, S. Münzer, S.-J. Lohmeier, A. Feldhoff, K. Huber and M. Wiebcke, *Chem. Mater.*, **21**, 1410 (2009).
39. M. Fang, C. Wu, Z. Yang, T. Wang, Y. Xia and J. Li, *J. Membr. Sci.*, **474**, 103 (2015).
40. S. Hwang, W. S. Chi, S. J. Lee, S. H. Im, J. H. Kim and J. Kim, *J. Membr. Sci.*, **480**, 11 (2015).

41. Y.-R. Lee, M.-S. Jang, H.-Y. Cho, H.-J. Kwon, S. Kim and W.-S. Ahn, *Chem. Eng. J.*, **271**, 276 (2015).
42. N. A. H. M. Nordin, A. Ismail, A. Mustafa, R. S. Murali and T. Matsuura, *RSC Adv.*, **4**, 52530 (2014).
43. R. L. Papporello, E. E. Miró and J. M. Zamaro, *Micropor. Mesopor. Mater.*, **211**, 64 (2015).
44. Y. Wang, Y. Xu, H. Ma, R. Xu, H. Liu, D. Li and Z. Tian, *Micropor. Mesopor. Mater.*, **195**, 50 (2014).
45. A. Jomekian, R. M. Behbahani, T. Mohammadi and A. Kargari, *Micropor. Mesopor. Mater.*, **234**, 43 (2016).
46. Y.-R. Lee, J. Kim and W.-S. Ahn, *Korean J. Chem. Eng.*, **30**, 1667 (2013).
47. J. Cravillon, C. A. Schröder, R. Nayuk, J. Gummel, K. Huber and M. Wiebcke, *Angew. Chem. Int. Ed. Engl.*, **123**, 8217 (2011).
48. S. Cao, G. Gody, W. Zhao, S. Perrier, X. Peng, C. Ducati, D. Zhao and A. K. Cheetham, *Chem. Sci.*, **4**, 3573 (2013).
49. E. L. Bustamante, J. L. Fernández and J. M. Zamaro, *J. Colloid Interface Sci.*, **424**, 37 (2014).
50. J. Cravillon, R. Nayuk, S. Springer, A. Feldhoff, K. Huber and M. Wiebcke, *Chem. Mater.*, **23**, 2130 (2011).
51. A. F. Gross, E. Sherman and J. J. Vajo, *Dalton Trans.*, **41**, 5458 (2012).
52. C.-W. Tsai and E. H. Langner, *Micropor. Mesopor. Mater.*, **221**, 8 (2016).
53. D. Yamamoto, T. Maki, S. Watanabe, H. Tanaka, M. T. Miyahara and K. Mae, *Chem. Eng. J.*, **227**, 145 (2013).
54. P. Zhang, F. Sun, Z. Xiang, Z. Shen, J. Yun and D. Cao, *Energy Environ. Sci.*, **7**, 442 (2014).
55. Y.-Y. Fu, C.-X. Yang and X.-P. Yan, *Chem. Commun.*, **49**, 7162 (2013).
56. L. G. Qiu, T. Xu, Z. Q. Li, W. Wang, Y. Wu, X. Jiang, X. Y. Tian and L. D. Zhang, *Angew. Chem. Int. Ed. Eng.*, **47**, 9487 (2008).
57. L.-B. Sun, J.-R. Li, J. Park and H.-C. Zhou, *J. Am. Chem. Soc.*, **134**, 126 (2011).
58. A. Jomekian, R. M. Behbahani, T. Mohammadi and A. Kargari, *J. Solid State Chem.*, **235**, 212 (2016).
59. J. H. Kim, S. Y. Ha and Y. M. Lee, *J. Membr. Sci.*, **190**, 179 (2001).
60. D. Zhao, J. Ren, H. Li, K. Hua and M. Deng, *J. Energ. Chem.*, **23**, 227 (2014).
61. K. Norrman, A. Ghanbari-Siahkali and N. B. Larsen, *Annual Reports Section "C" (Physical Chemistry)*, **101**, 174 (2005).
62. P. Burmann, B. Zornoza, C. Téllez and J. Coronas, *Chem. Eng. Sci.*, **107**, 66 (2014).
63. Y. Shen and A. C. Lua, *Chem. Eng. J.*, **188**, 199 (2012).
64. A. Bondi, *J. Phys. Chem.*, **68**, 441 (1964).
65. D. Hua, Y. K. Ong, Y. Wang, T. Yang and T.-S. Chung, *J. Membr. Sci.*, **453**, 155 (2014).
66. M. A. Aroon, A. F. Ismail, T. Matsuura and M. M. Montazer-Rahmati, *Sep. Purif. Technol.*, **75**, 229 (2010).
67. A. F. Ismail and W. Lorna, *Sep. Purif. Technol.*, **27**, 173 (2002).
68. C. P. Ribeiro, B. D. Freeman and D. R. Paul, *J. Membr. Sci*, **377**, 110 (2011).
69. Y. Li and T.-S. Chung, *Int. J. Hydrogen Energy*, **35**, 10560 (2010).
70. F. Dorosti, M. Omidkhah and R. Abedini, *Chem. Eng. Res. Des.*, **92**, 2439 (2014).
71. F. Dorosti, M. Omidkhah and R. Abedini, *J. Nat. Gas Sci. Eng.*, **25**, 88 (2015).
72. R. Mahajan and W. J. Koros, *Polym. Eng. Sci.*, **42**, 1420 (2002).
73. R. Mahajan and W. J. Koros, *Polym. Eng. Sci.*, **42**, 1432 (2002).
74. T. T. Moore, R. Mahajan, D. Q. Vu and W. J. Koros, *AIChE J.*, **50**, 311 (2004).
75. D. Q. Vu, W. J. Koros and S. J. Miller, *J. Membr. Sci.*, **211**, 311 (2003).